JOURNAL OF BACTERIOLOGY, June 1983, p. 1414–1430
0021-9193/83/061414-17$02.00/0

Vol. 154, No. 3

Spatial Differentiation in Photosynthetic and Non-Photosynthetic Membranes of *Rhodopseudomonas palustris*

AMY R. VARGA* AND L. ANDREW STAEHELIN

Department of Molecular, Cellular and Developmental Biology, University of Colorado, Boulder, Colorado 80309

Received 12 November 1982/Accepted 15 March 1983

The cytoplasmic membrane and the photosynthetic intracytoplasmic membranes of *Rhodopseudomonas palustris* are spatially differentiated into regions of extremely high intramembrane-particle density (4,400 to 9,800/μm^2) and areas of lower intramembrane-particle density (2,700 to 5,900/μm^2). The high intramembrane-particle-density areas were always seen in association with photosynthetic membrane stacks. This differentiation was also seen in those areas of the cytoplasmic membrane which adhere to the underlying intracytoplasmic membranes, implying that the cytoplasmic membrane too is differentiated for photosynthesis in these regions. Changes in intramembrane-particle size distribution in response to changes in light intensity during growth were measured. We found that, as light levels were decreased from 8,500 to 100 lx, the average particle diameter in the protoplasmic face of stacked intracytoplasmic and cytoplasmic membranes increased from 8.6 to 10.3 nm. We also observed a distinct periodicity in the sizes of the intramembrane particles found in the stacked regions—7.5, 10.0, 12.5, and 15.0 nm—with the larger-size peaks becoming more pronounced as light intensity decreased. This suggests that, as light levels decrease, subunits of discrete size are being added to a core particle. A comparison of propane jet-frozen cells versus fixed, glycerinated, and then frozen cells indicated that ultrarapid freezing leads to a higher quality of fine-structure preservation than does chemical fixation followed by glycerination and conventional freezing in Freon-12 or propane. The intramembrane particles appeared to be more regular in size, lacking the deformed or jagged appearance displayed in fixed preparations.

Rhodopseudomonas palustris provides an excellent procaryotic system for the study of membrane differentiation. Like many other *Rhodospirillaceae*, *R. palustris* is a facultative photoheterotroph, capable of respiration under aerobic conditions and photosynthesis under anaerobic light conditions (5, 17, 32). In the photosynthetic mode of growth, the cells exhibit infoldings of the cytoplasmic membrane (CM) which extend into the cell in the form of characteristic stacks of flattened thylakoid membrane sacks (47, 52). These thylakoids, termed intracytoplasmic membranes (ICMs), contain the pigment proteins and other components associated with photosynthetic activity in these cells (5, 17, 18). The synthesis of the ICMs and the components of the photosynthetic apparatus is controlled by the oxygen partial pressure in the growth medium; low oxygen levels induce the formation of the photosynthetic membranes (8, 18). The amount of ICM present by weight in the photosynthetic cell is regulated at a secondary level by light intensity. High light intensities during growth yield cells with small arrays of ICM, whereas low light intensity induces more extensive ICM synthesis (8, 37). The mechanics of ICM differentiation have recently been reviewed in detail by Drews (5), Kaplan (17, 18), and Kaplan and Arntzen (19).

The photosynthetic apparatus of *R. palustris* is made up of three major pigment proteins which can constitute up to 80% of the ICM by weight (29). These components are the reaction center (RC), light-harvesting component I (LHI) B875, and light-harvesting component II (LHII) B800-850. The RC and LHI are found in a relatively constant stoichiometric ratio, whereas LHII varies, relative to the RC, inversely in proportion to light intensity. That is, the lower the light intensity, the more LHII per RC is synthesized (8). Changes in the ratios of the RC, LHI, and LHII can be monitored spectrophotometrically since these components have characteristic absorption peaks.

The thylakoids of *R. palustris* resemble algal and higher plant thylakoids, at least at a gross morphological level. Thin-section electron microscopy shows that chloroplast thylakoids are

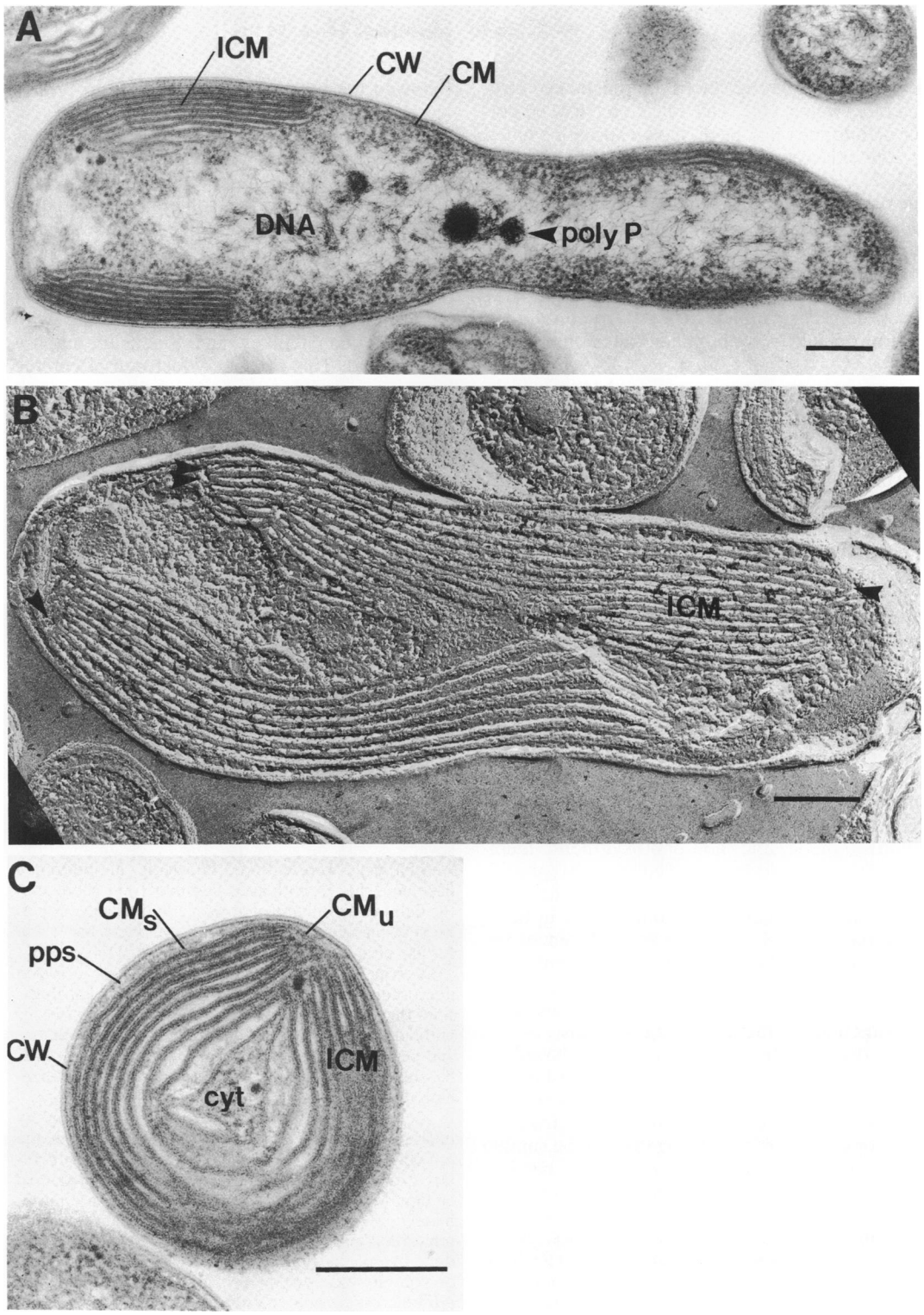

FIG. 1. Photosynthetic *R. palustris* cells grown at 900 lx. (A) Longitudinal section of a cell in which large stacks of ICM, the CM, and the cell wall (CW) are clearly resolved. Polyphosphate (poly P) granules and DNA are visible in the central region of the cell. At the right, smaller arrays of ICM are seen in the budding daughter cell. Bar, 0.2 μm. (B) Longitudinal cross-fracture of a jet-frozen cell containing very large stacks of ICM, the ends of which (arrowheads) are seen to be closed. Bar, 0.2 μm. (C) Cross-section of a cell. The ICMs are arranged in a stack around the cell periphery with a small amount of cytoplasm (cyt) visible in the center. The rather wide periplasmic space (pps) is filled with lightly staining material. A small area of CM_u is seen where the two ends of the ICM stack meet. Bar, 0.2 μm.

separated into grana stacks and unstacked stroma membranes (44). The adhesion between grana membranes has been shown to be mediated by the chlorophyll *a/b* light-harvesting complex (22, 27). A similar tight appression of stacked membranes was also observed in *R. palustris* (Fig. 1), but nothing is known about the mechanism of adhesion or the molecule(s) which promotes this type of membrane association. The bottom (unappressed) membrane of an ICM stack may correspond, at least structurally, to the unstacked stroma membranes in chloroplasts.

Both morphological and biochemical techniques were used to analyze the structural and functional differentiation of chloroplast thylakoids associated with the stacked (grana) and unstacked (stroma) membrane regions. In terms of detailing the structural differentiation of photosynthetic membranes, freeze-fracture electron microscopy has proven to be the most informative approach. This method provides a means for visualizing individual functional membrane complexes in the form of discrete intramembrane particles (IMPs), and in recent years, considerable progress has been made in correlating specific size classes of particles with functional units in the thylakoid membrane (19, 42). The goals of the present study were to extend the understanding of the structural correlations with function in the procaryotic photosynthetic membrane of *R. palustris* in the following ways: (i) to see whether structural differences between photosynthetic and non-photosynthetic membrane areas could be resolved, thereby providing a means for mapping the distribution of photosynthetic membrane components in these bacteria; (ii) to characterize any differences between appressed and nonappressed membranes of the thylakoid stacks; (iii) to correlate any structural differentiation with possible biochemical functions of the membrane systems.

As the main thrust of this work is based on electron microscopy, it is important to keep in mind some of the caveats of the techniques involved. One problem inherent in electron microscopy is that of stabilizing (fixing) the sample for examination in the microscope. Chemical fixatives achieve this end, but they do not act instantaneously and so allow time for artifactual rearrangements of cellular components. A recent study indicated that it may take 6 to 9 s for a 3% glutaraldehyde solution to fix a one-cell-thick capillary wall (J. Boyles, N. L'Hemault, H. Laks, and G. E. Palade, J. Cell Biol. **91**:418, 1981, no. 24048), which is ample time for membrane lipids or proteins to diffuse the entire length of a bacterial cell (9, 36). Most of the past freeze-fracture work has been done with the sample first subjected to glutaraldehyde fixation followed by infiltration with glycerol to reduce ice crystal formation during freezing (13, 21, 24, 34). Both the fixation and cryoprotection steps can produce artifacts of membrane structure in bacteria (27), as well as in plant and animal cells (34), making these steps sometimes unsatisfactory for fine-structure analysis of membranes. In the present study, we tried to circumvent these problems by a method of ultrarapid freezing using a propane jet freezer (20). Cooling rates of approximately −10,000°K/s are possible with this apparatus (Gilkey and Staehelin, unpublished data). This extremely fast rate of cooling fixes the cells instantly and reduces ice crystal formation to a minimum, thus eliminating the need for either glutaraldehyde or glycerol with their possible artifacts. The ultrarapid freezing method used produces a more accurate picture of cellular architecture than is possible with more conventional specimen preparation techniques and, therefore, is our preferred method of cell preservation.

MATERIALS AND METHODS

Cells and culture conditions. The cells used were *R. palustris* 1e5, a gift from Gerhart Drews, Freiburg, Germany. The cells were grown in a phosphate-buffered malate medium with 0.1% yeast extract added. Photosynthetic cells were cultured in completely filled 250-ml screw-top bottles at 28 to 30°C, illuminated by four 15- or 100-W incandescent light bulbs at 900 or 8,500 lx, respectively, or four 15-W bulbs shielded by several layers of gauze for 100 lx of illumination. Aerobic cells were cultured in a large, flat-bottomed flask on a shaker, with air (140-mm pO_2) bubbling into the culture, and illuminated with a fluorescent lamp to prevent pigment synthesis. The cells were harvested for use at a culture optical density at 650 nm of 0.6.

Electron microscopy. The cells used for electron microscopic analysis were harvested by centrifugation, then ultrarapidly frozen by a propane jet freezer without prior fixation or glycerination. Freeze-fracture and platinum-carbon replication were done at −104°C by standard procedures, using a Balzers 360 freeze-etch device.

The cells were prepared for thin sectioning by fixation with 0.5% glutaraldehyde for 45 min in the growth medium, washed, and then postfixed with 1% OsO_4 for 1 h. The cells were washed and then stained en bloc with 0.5% aqueous uranyl acetate for approximately 18 h at 4°C. Dehydration in acetone and infiltration and polymerization with Spurrs resin were done by standard procedures. Silver interference-color sections were cut on an American Optical-Richert ultramicrotome with a SAG International or Du Pont diamond knife. The sections were stained with a lead stain containing three lead salts (35) for 3 min.

All samples were examined in a JEOL/JEM 100C microscope at 80 kV or a Hitachi H-600 at 75 kV.

Membrane isolation. Photosynthetic membranes were isolated by homogenizing whole cells with glass beads for 20 min at 4°C in a Virtis homogenizer. Whole

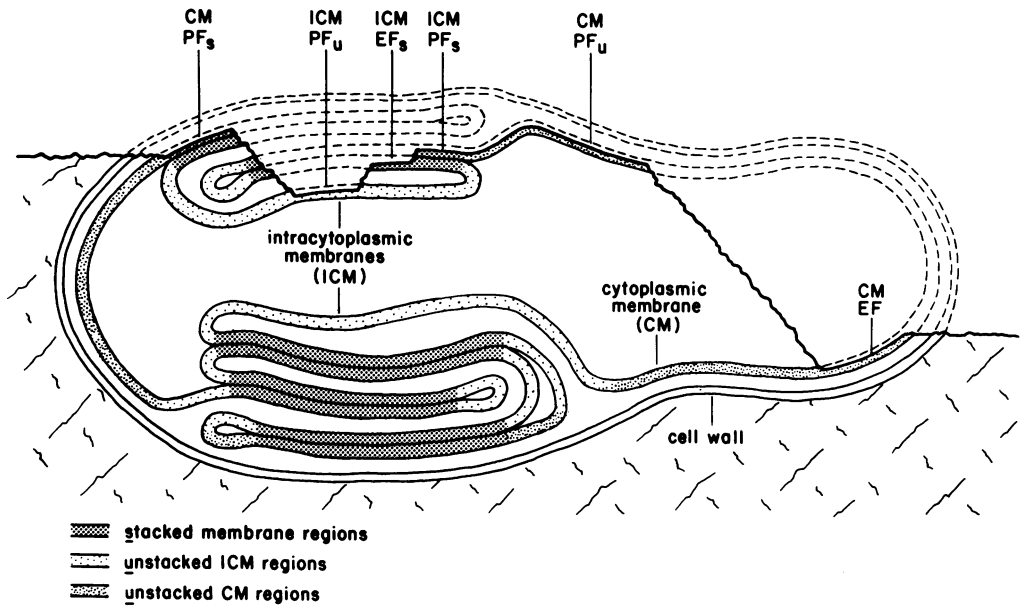

FIG. 2. Diagram illustrating the nomenclature for the freeze-fractured membranes of *R. palustris*.

cells, cell wall fragments, and glass beads were pelleted (1,000 × *g*) and discarded. The pellet from an 11,000 × *g* centrifugation contained large pigmented vesicles and thylakoids. The pellet from a 30,000 × *g* centrifugation contained a clear suspension of small pigmented vesicles, which were used for spectroscopy.

Analytical methods. (i) Particle measurements. Membrane fracture faces were labeled by the nomenclature of Branton et al. (1). For measurements, 200,000× enlargements were used, and IMPs were measured by the method of Staehelin (42). A minimum of 500 particles were measured for each fracture face from several cell preparations. The particle densities were determined by counting the number of particles on each fracture face within a 1-μm^2 grid.

(ii) Spectroscopy. Bacteriochlorophyll (Bchl) was determined by the method of Cohen-Bazire et al. (4). Absorption spectra were taken from membrane fragments (30,000 × *g* pellet) of cells grown at 100, 900, and 8,500 lx with a Perkin-Elmer 360 UV/vis-near-infrared spectrophotometer (1-cm path length).

RESULTS

General morphology. En bloc staining with uranyl acetate (0.5% aqueous) gives excellent resolution of membranes relative to other cellular structures (Fig. 1A and C). The images thus obtained indicate that photosynthetic membranes are appressed to one another in the ICM stacks and also where the ICMs abut against the CM (Fig. 1A to C). The appression of the ICM and the CM is also apparent in cross-fractured freeze-etch preparations, and the closed ends of the ICM sacks are seen (Fig. 1B). The arrangement of the ICMs around the periphery of the cell and the appression to the CM are most readily seen in cross-section views (Fig. 1C). The clear spaces in the ICM stack are the luminal spaces of the ICM sacks. The lumen may be contiguous with the periplasmic space, as connections from the ICM to the CM can occasionally be resolved (see Fig. 3A).

The uranyl acetate staining procedure also clearly reveals polyphosphate (6, 22) and DNA in the central region of the cell (Fig. 1A; see also Fig. 3A). Another feature observed is the staining of material in the periplasmic space, between the CM and the outer cell wall membrane (Fig. 1A and C; see also Fig. 3A). This material is not as readily apparent with other preparation procedures (21, 52), and the composition of the stained material is unknown.

When subjected to mechanical stress, frozen cell membranes split between the halves of the bilayer, revealing the hydrophobic inner surface of the membrane leaflets (2). The leaflets, or fracture faces, are labeled according to their proximity to either the protoplasm, P-face (PF), or the exoplasm, E-face (EF), as explained by Branton et al. (1). Figure 2 represents a *R. palustris* cell with the fracture faces labeled; the different types of fracture faces (s, stacked; u, unstacked) are documented in Fig. 3 to 7.

Invaginations connecting the CM with the ICM were seen in photosynthetically growing

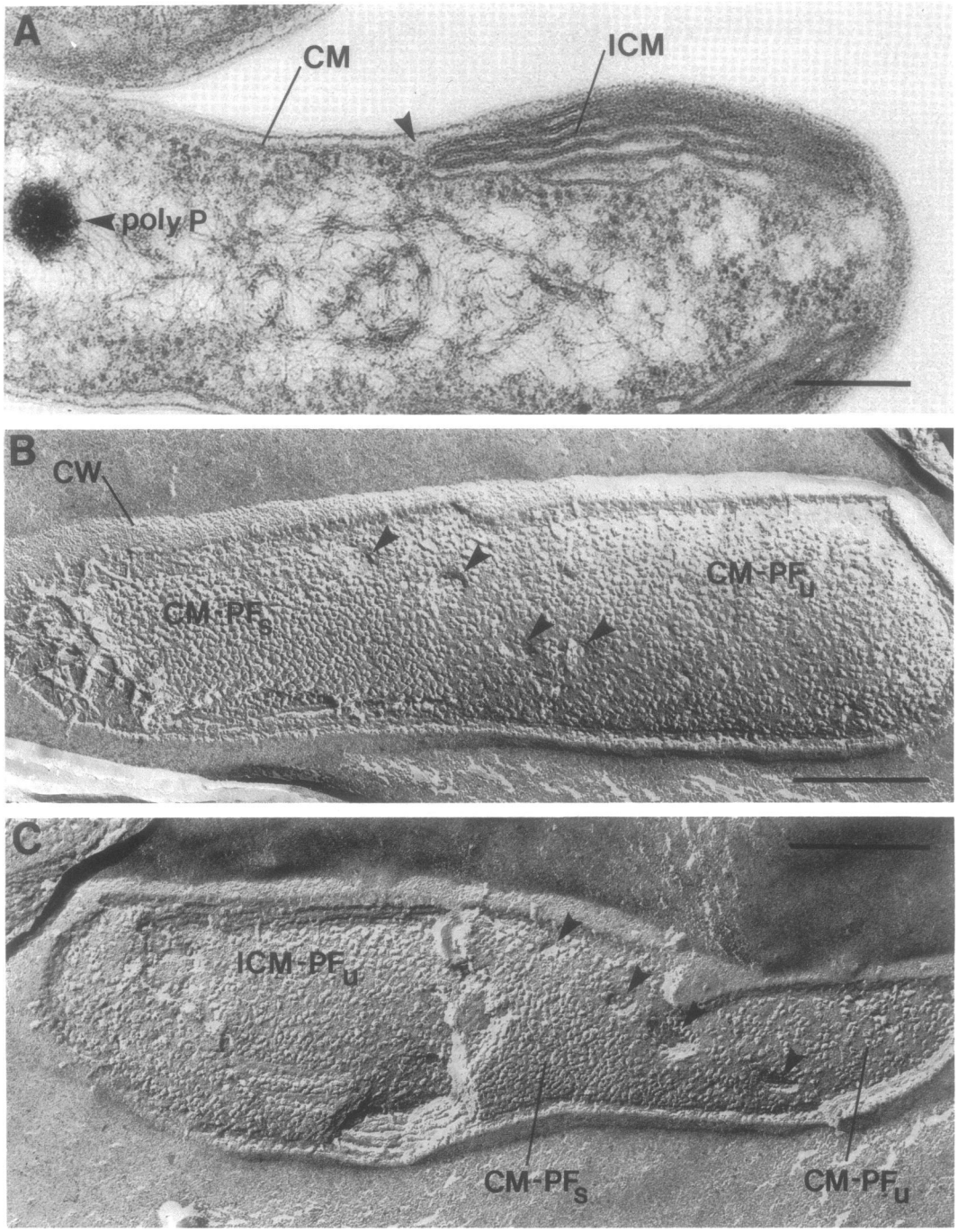

FIG. 3. Electron micrographs of photosynthetic *R. palustris* cells grown at 900 lx. (A) Longitudinal section showing how the CM is connected to the ICM (arrowhead). poly P, Polyphosphate. Bar, 0.2 μm. (B) PF view of the CM of a jet-frozen cell. The invaginations (arrowheads) correspond to regions where the CM is continuous with the ICM as shown in (A). The typical differentiation of the CM into PF_s and PF_u regions is clearly seen. Bar, 0.2 μm. (C) PF views of the CM and ICM of a jet-frozen cell. The arrowheads point to invaginations of the CM. The PF_s and PF_u regions of the CM are labeled. On the left, the fracture plane passes from the cell surface through the entire ICM stack to the bottom, unstacked membrane. Bar, 0.2 μm.

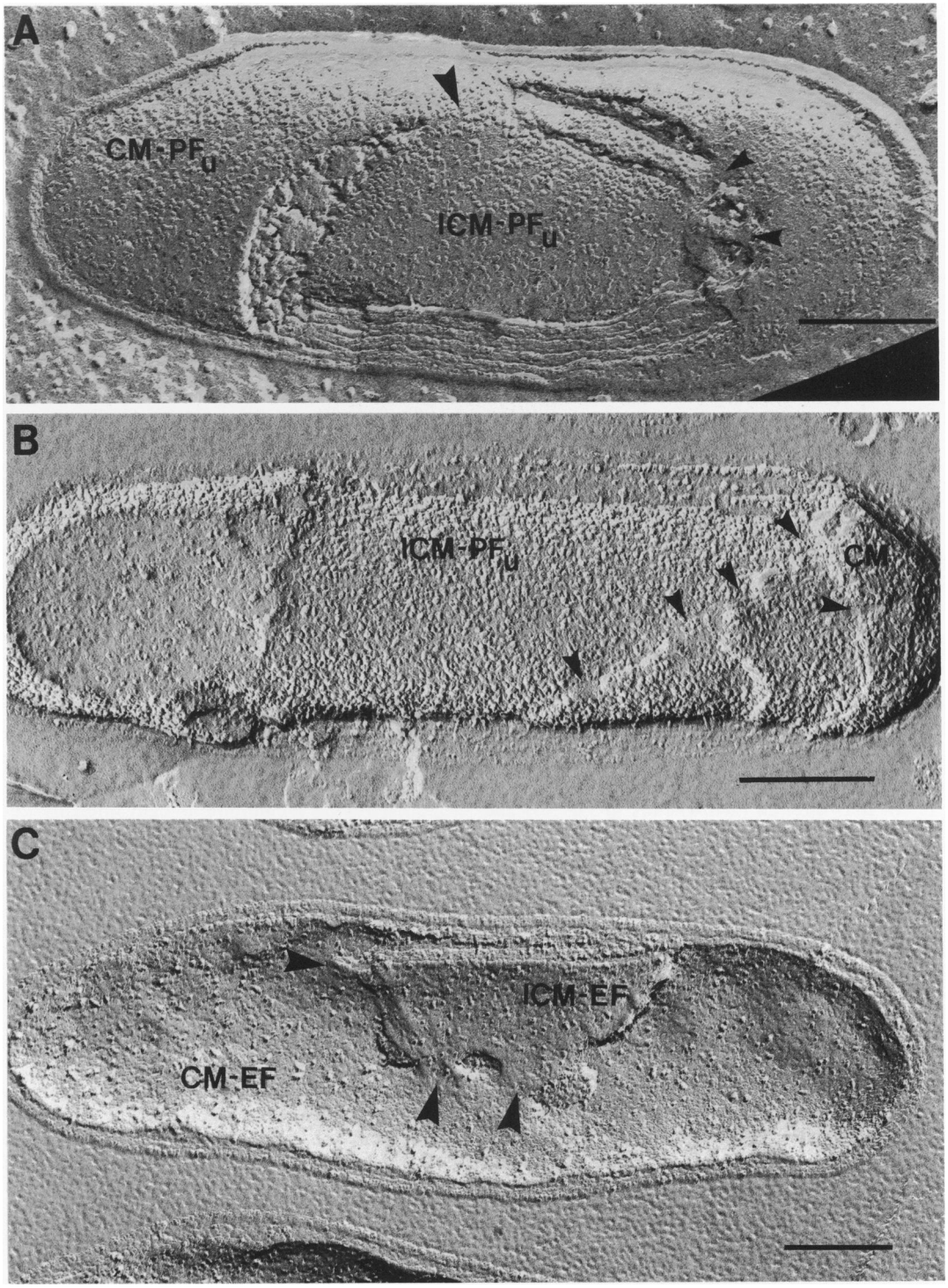

FIG. 4. Photosynthetic cells of *R. palustris* grown at 900 lx. (A) PF view of the CM and ICMs of a jet-frozen cell illustrating the physical continuity of the two membrane systems (arrowheads). The fracture plane goes from the CM-PF$_u$ to the bottom ICM-PF$_u$. Bar, 0.2 μm. (B) PF view of the CM and ICMs of a cell fixed with glutaraldehyde and glycerinated before freezing. Note the jagged appearance of the particles in comparison with those in (A). Membrane connections are shown by arrowheads. Bar, 0.2 μm. (C) EF view of the CM and a small ICM stack of a glutaraldehyde-fixed cell. The multiple, flattened tubular connections between the CM and the bottom ICM are clearly resolved (arrowheads). Bar, 0.2 μm.

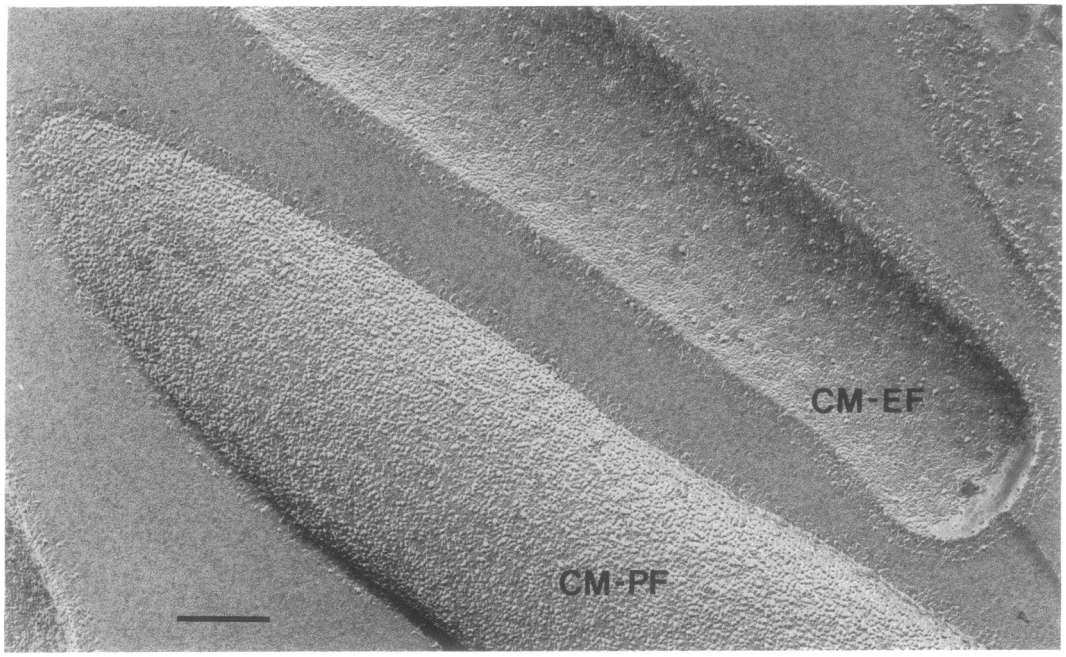

FIG. 5. Aerobic *R. palustris* cells grown at 140-mm pO_2. PF and EF views of a glutaraldehyde-fixed cell are shown; note the lack of invaginations in the CM. Bar, 0.2 μm.

cells. This is illustrated in Fig. 3A. On the CM-PF of fractured cells, these connections are detected as roughly C-shaped indentations going down into the cell (arrowheads in Fig. 3B and C); on the CM-EF, protrusions are seen where the ICMs have been broken away from the remainder of the cell (Fig. 7B). Occasionally, the fracture plane follows the membranes through an invagination, and a clear connection between the ICM and the CM can be seen (Fig. 4A to C). In aerobically grown cells no ICMs are made, and no invaginations of the CM are observed (Fig. 5). Figure 8 summarizes several features observed in the electron microscope and diagrams the spatial relationship of the cell wall, CM, and ICMs.

A comparison of fixed with jet-frozen samples shows that the IMPs of the fixed cells are irregular and jagged in shape as though small bits of material were stuck to them or they were deformed during the fracturing process (Fig. 4B and C). Jet-frozen, as well as unfixed but glycerinated, samples have regular, more smooth-appearing IMPs (Fig. 3B and C, 4A, 6, 7), but glycerination appears to reduce the number of CM-ICM connections (Staehelin, unpublished data). Jet-freezing also has the advantage of an aqueous medium, which is much more amenable to deep-etching, which reveals membrane surfaces without leaving a latticework of glycerol behind.

Membrane area, pigment content. Ratios of linear tracings of nonappressed CM to ICM and appressed CM clearly indicate the increase of photosynthetic membrane as light intensity decreased (Table 1). At the lowest light intensity (100 lx), the ICM/CM ratio was 3.15, indicating that the surface area of the ICMs is approximately three times that of the CM. At 8,500 lx, the ICM/CM ratio decresed to 0.76, indicating 25% less ICM than CM area. The aerobically grown cells show no evidence of ICM (Fig. 5), and no pigment is detectable. These light-dependent changes in the ICM/CM ratio were paralleled by changes in the Bchl concentration (Table 1).

The absorbance spectra of membrane fragments are indicative of changes in the photosynthetic apparatus as light levels were varied. At low light levels, there was significantly more LHII, indicated by the large absorbance peak at 805 nm (Fig. 9, solid line). As light is increased, LHII decreases relative to the RC-LHI peak, 865 to 875 nm (Fig. 9, dotted lines). In contrast, the absorbance in the carotenoid region increases greatly as light intensity is increased. This is consistent with the observation that carotenoids serve a protective function for photooxidation, as well as acting as antenna pigments associated with the RC (3, 38). The absorbance increase may simply reflect the relative increase in the RC or an increase in the carot-

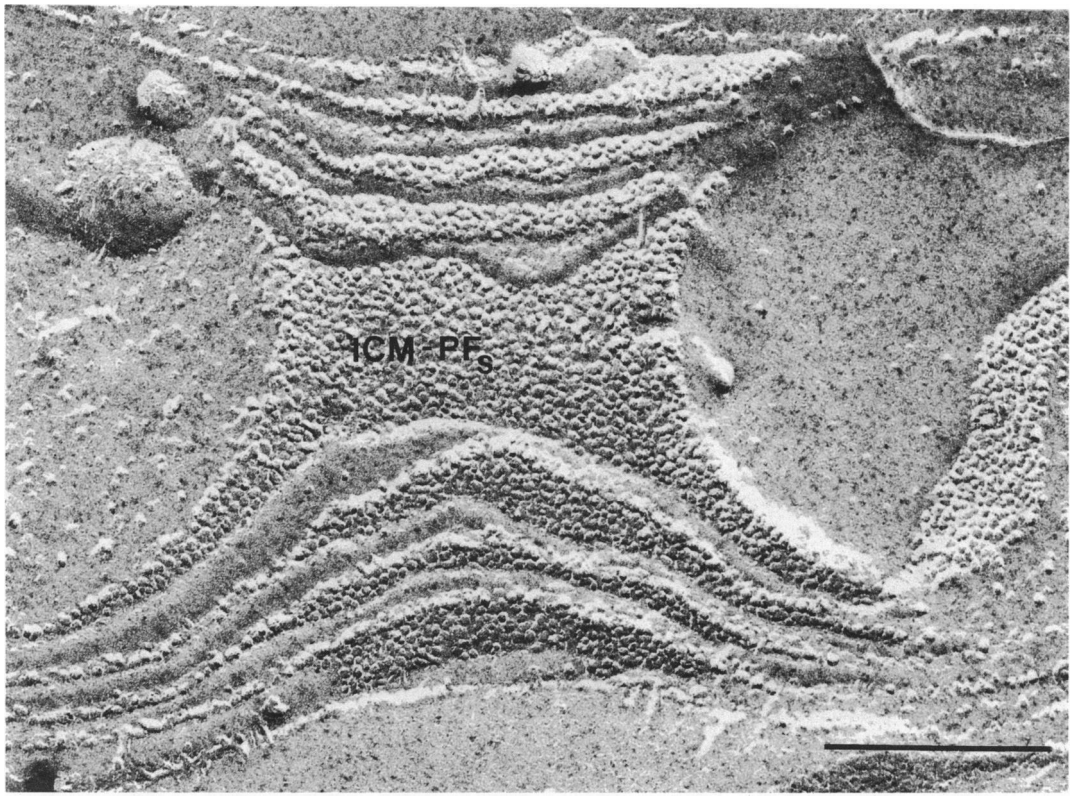

FIG. 6. Photosynthetic *R. palustris* cell grown at 900 lx. A PF_S view of adherent membranes of an ICM stack of a jet-frozen cell is shown. The close-packing of particles is evident. Bar, 0.2 μm.

enoid content of LHI at higher light levels; our results do not allow us to determine the precise reason for the carotenoid increase.

Freeze-fracture morphology of the membranes. In photosynthetic cells, PF views of the CM reveal a mosaic-like structure of particles, with very high particle density areas lying adjacent to areas of lower particle density (Fig. 3B and C). The high-particle-density areas are most often seen bounded by invaginations of the CM which connect to the membranes of the ICM stacks (arrows in Fig. 3B and C, 7B). When a fracture plane goes through a high-particle-density area and continues into the cell, ICMs are seen underneath the CM (Fig. 3C, 7A). These observations were made at all light levels tested, thus suggesting that the distribution of particles in the CM is affected by adjacent, underlying ICMs.

When the plane of fracture goes through the central part of the ICM stack, areas of high particle density are seen in the PFs of these photosynthetic membranes (Fig. 6). That is, the ICMs in the internal part of the stack which are appressed together exhibit the same high particle density as do the adjacent CM regions. In contrast, the bottom, unappressed membrane of the ICM stack has a lower particle density (Fig. 3C and 4A), a distribution much like that of the unappressed regions of the CM. Table 1 summarizes the particle density values of the various fracture faces at all light levels and for aerobically grown cells.

A decrease in the light level at which anaerobic *R. palustris* cells were cultured led not only to an increase in the ICM/CM ratio, but also to an increase in the average size of the IMPs and to changes in the size class distribution of the particles. These latter changes are particularly evident on the PF of appressed, or stacked, membranes of the CM and ICMs. Particle size histograms for all membrane faces under all growth conditions are illustrated in Fig. 10 and 11. Of particular interest for the current study are the PF histograms for the stacked membrane regions of the CM and ICM (Fig. 10B and D). At the lowest light level (100 lx), the CM-Pf_Sdistribution is trimodal, with peaks centered at 7.5, 10.0, and 12.5 nm; the ICM-PF_S distribution is tetramodal, with peaks centered at 7.5, 10.0, 12.5, and 15.0 nm. As light levels increase, the

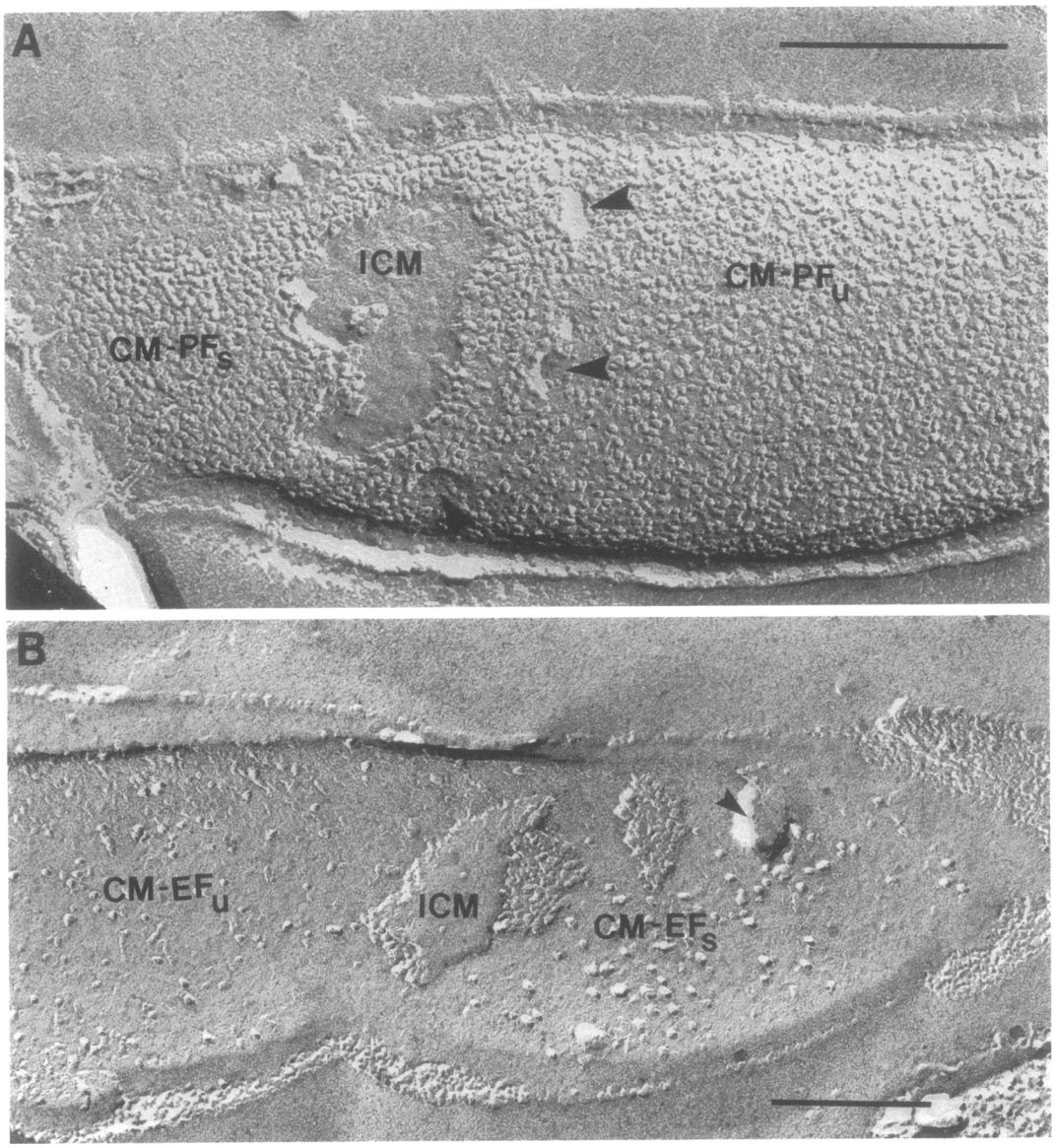

FIG. 7. Photosynthetic *R. palustris* cells grown at 8,500 and 100 lx. (A) PF view of an 8,500-lx-grown cell that was jet frozen. The arrowheads indicate connections between the CM and underlying ICMs. CM-PF_s is seen with ICM-EF_s underneath. Bar, 0.2 μm. (B) EF view of a 100-lx-grown cell that was jet frozen. The view shown is complementary to that in (A). In this picture, the CM-ICM connecting region appears as an evagination of the CM. CM-EF_s is seen with remnants of ICMs on top. Bar, 0.2 μm.

peaks for the larger particle sizes diminish, whereas those for the smaller sizes increase, until at 8,500 lx there is basically a bimodal distribution for both the CM and ICM, with peaks centered at 7.5 and 10.0 nm only. The striking feature of these histograms is the distinct periodicity of the PF_s particle sizes (2.5 nm) and the similarity and parallel change of the ICM-PF_s and CM-PF_s histograms at different light levels.

At low light levels (100 lx), two regions of the CM EF can be detected. In areas where the ICM stack has been pulled away from the CM, exposing the EF, areas of very large EF particles are revealed, strikingly different in size from those in the remainder of the CM-EF (Fig. 7B and

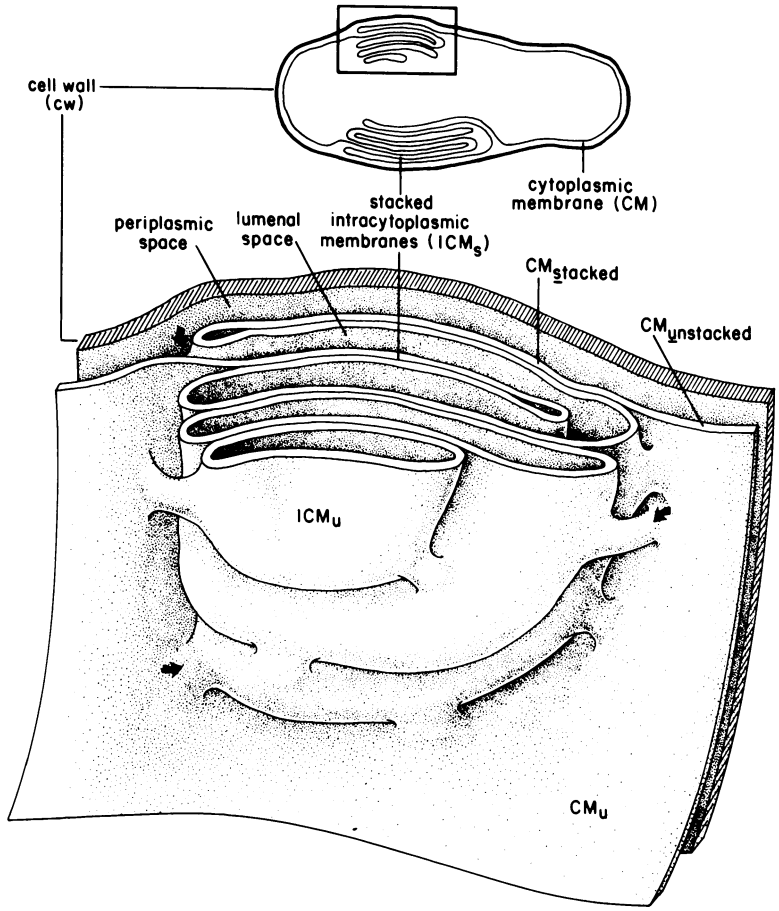

FIG. 8. Drawing showing the spatial relationship between the cell wall, CM, and ICMs as revealed in this study. Tubular connections between the CM and ICMs at different levels of the stack, as well as between adjacent ICMs, are shown. A cross-section of a membrane connection is illustrated at the upper left.

11D). The size classes of these large particles are nearly identical with the CM-PF_s and ICM-PF_s (cf. Fig. 10B and D and 11D). At higher light intensities, the differences between the two CM-EF regions are less evident, possibly because at 100 lx, the particles in the stacked CM regions are quite large and partition more readily with the EF than do the smaller particles in cells grown at higher light levels.

The PF histograms of the unstacked (nonappressed) region of the CM of photosynthetic cells (Fig. 10A) appear similar to the CM-PF profile of the aerobic cells (Fig. 11C). This correlates with the evidence that aerobic cell and photosynthetic cell CMs (unappressed) are similar in composition (31, 51).

It is evident that as light levels increase, overall particle density increases along with a decrease in average particle diameter (Table 1). If aerobic cell membrane particle density is taken as a control value, overall particle densities (as a percent control value) were 61% (100 lx), 79.5% (900 lx), and 131.8% (8,500 lx) for the PF of the nonappressed CM. For the corresponding EF, the values were 66% (100 lx), 99% (900 lx), 109.9% (8,500 lx).

Perhaps a more significant comparison is one which takes into account the change in average particle size, as well as particle density, as growth conditions are varied. By calculating the circular area of a single mean-size particle and multiplying this area by the number of particles per square micrometer, one can determine the membrane surface area actually occupied by IMPs in a square micrometer (the remaining area is lipid bilayer). The IMP surface area values are given in Table 2. It can be seen that for the CM-EF, the values were very similar under all

TABLE 1. Summary of freeze-fracture data for PFs

Membrane face	Particle density (per μm^2)				Mean particle size (nm) ± SEM			
	100 lx	900 lx	8,500 lx	Aerobic cells	100 lx	900 lx	8,500 lx	Aerobic cells
CM-PF_s	4,200	6,500	9,800		10.1 ± 0.106	9.9 ± 0.079	8.9 ± 0.067	
ICM-PF_s	4,400	6,700	8,800		10.3 ± 0.113	9.4 ± 0.081	8.6 ± 0.063	
CM-PF_u	2,700	3,500	5,800	4,400	8.0 ± 0.084	8.2 ± 0.095	7.5 ± 0.063	7.6 ± 0.085
ICM-PF_u	3,200	3,600	5,900		9.4 ± 0.115	9.2 ± 0.079	8.4 ± 0.067	
ICM/CM surface area	3.15	2.28	0.76					
Bchl/cell wt (mg/g)	0.62	0.57	0.25					

growth conditions, indicating that even though particle density increases with increasing light, the actual area occupied by protein particles in the bilayer which partitions into the EF remains fairly constant. This does not hold true for the CM-PF_u or the stacked regions of either the CM or ICM. Proteins are inserted into membranes from the cytoplasmic side and usually remain functionally biased toward this side. This bias is reflected by the generally higher IMP density of P-fracture faces of nearly all types of membranes of both procaryotic and eucaryotic cells (13, 14, 24, 33, 42–45); it is therefore logical to assume that changes in membrane protein composition are primarily seen in the PF particles. In these areas, particle density increased at such a rate that, despite a drop in the mean particle size, increasingly more membrane area was taken up by protein as light was increased. The area occupied by particles in the CM-PF increased 90 to 95% as light levels increased; for the ICM-PF, the increase was 70 to 75%. These changes appear to be related to the general increase in cellular activities at increasing light levels. Cells grown in high light have been shown to be more efficient in ATP production and to function at a higher metabolic rate than low-light-grown cells (32).

DISCUSSION

In most species of the *Rhodospirillaceae*, the photosynthetic apparatus is thought to be contained entirely in the ICM, with little or no evidence of extensive differentiation of the CM into a photosynthetic membrane (30, 31, 39). This does not seem to be the case for *R. palustris*. The stacked, or appressed, region of the CM is nearly identical to the ICM in freeze-fracture morphology: particle density, average

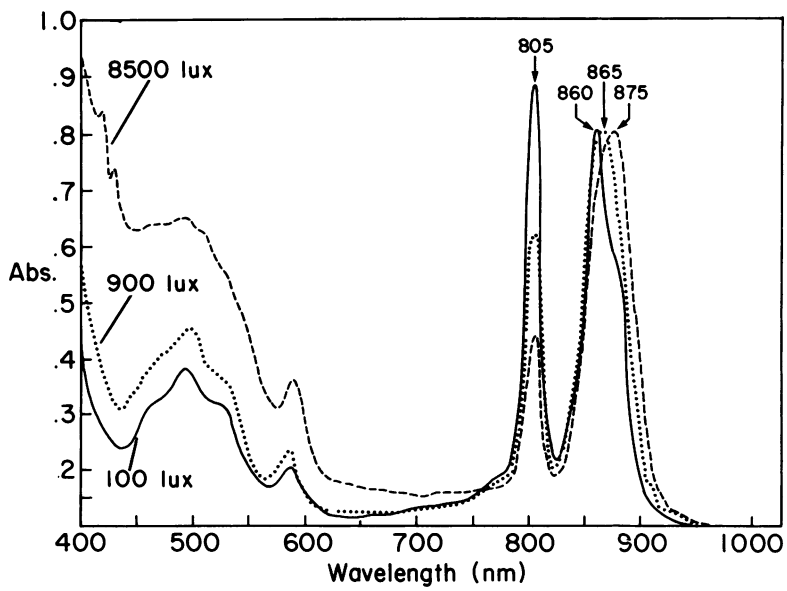

FIG. 9. Absorbance spectra of cells grown at 100, 900, and 8,500 lx.

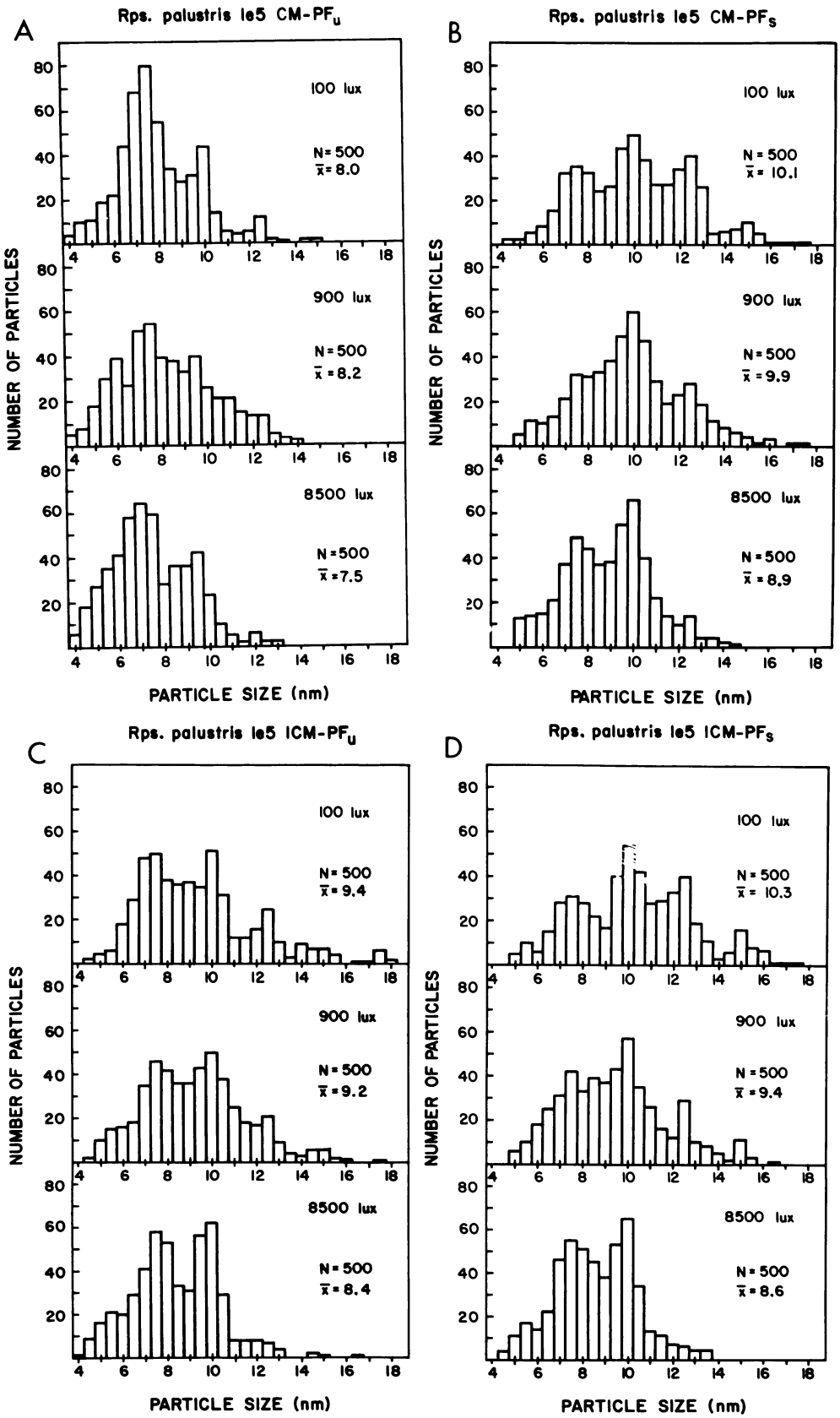

FIG. 10. Particle size histograms of photosynthetic *R. palustris* cells.

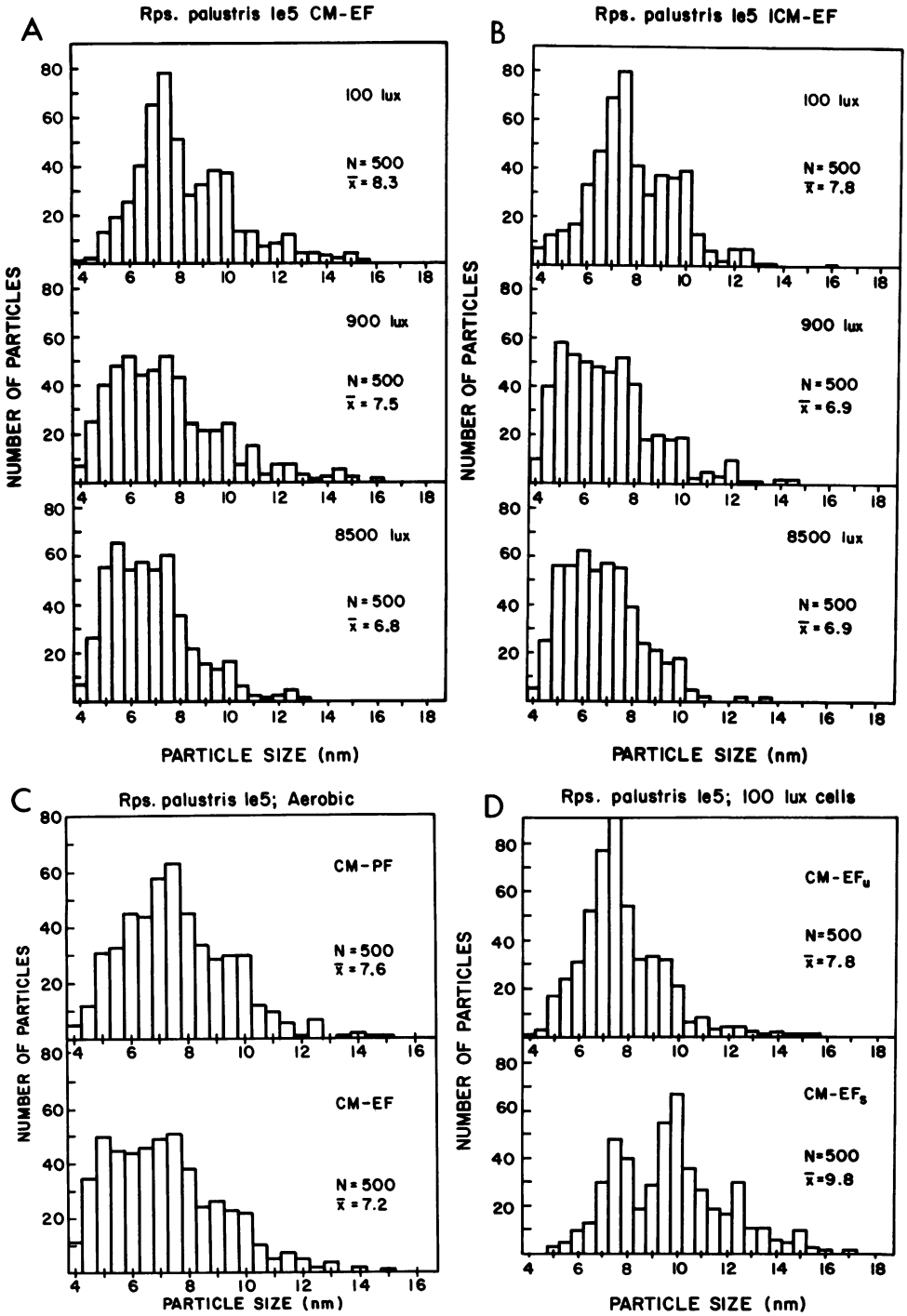

FIG. 11. Particle size histograms of photosynthetic (A, B, and D) and aerobic (non-photosynthetic; C) cells of *R. palustris*.

particle size, and most significantly, particle size distribution are essentially identical and vary in the same manner when light levels are changed. There is not simply an overall increase in particle size in the PF_s areas of the CM when light is decreased, as seems to be the case for the CM-PF_u areas. Instead, a specific change in clearly defined particle size classes is observed, exactly

TABLE 2. Mean membrane surface area occupied by IMPs

Growth condition	Mean membrane surface area (%)[a] occupied by IMPs on:				
	CM-PF_u	CM-PF_s	CM-EF	ICM-PF_u	ICM-PF_s
Aerobic	19.9		3.7		
100 lx	13.6	33.6	3.2	22.2	36.7
900 lx	20.3	50.0	4.0	23.9	46.5
8,500 lx	25.6	61.0	3.6	32.7	51.1

[a] Calculated using mean particle size and particle density for each membrane face.

the same classes which vary in the ICM where known, light level-dependent changes in the photosynthetic apparatus take place. Although this tight correlation between the two membrane systems does not prove that the CM is differentiated for photosynthesis in large areas, all of our findings are fully consistent with this interpretation. This idea is further supported by a recent report (49) which showed that antibodies against the RC of *R. sphaeroides* R-26 label the CM of this organism, as well as the ICMs. This may be significant in that *R. sphaeroides* R-26 has lamellar ICMs (21) and perhaps structural similarity to *R. palustris*.

It has been shown for *R. palustris* that the molar ratio of RC Bchl to LHI Bchl remains relatively constant, whereas the amount of LHII varies with the light level (8). We propose that the variation in particle size classes seen in the P-fracture faces of the ICM (PF_s and PF_u) and the CM-PF_s is directly related to the light level-dependent changes in the photosynthetic unit size. At high light intensities, the RC-LHI complex predominates; this is reflected by the absorbance spectrum of these cells with the large 875-nm peak (Fig. 9) and the smaller average particle size in the photosynthetic membranes (8.4 to 8.9 nm). When the light intensity is decreased, more LHII is put into the membranes as shown by the increase in the 805-nm absorbance peak (8, 15, 30, 37). Our particle size histograms reveal that this increase in LHII in the membranes is paralleled by an increase in the diameter of the average particle (9.4 to 10.1 nm) in the photosynthetic membranes.

Particle density is also affected by the change in particle size in that as particle size increases, particle density decreases, although the particles in the stacked regions are very close packed in all cases. When the increases in the ICM surface area are considered in conjunction with the changes in the other three parameters discussed above, we find that the particles occupy less of the membrane area, on the average, in low-light cells than in high-light cells (Table 2), indicating a drop in cell activity. Light level-dependent changes in particle size and density are also observed in the presumed non-photosynthetic CM regions. The overall changes suggest that the decrease in metabolic activity in low-light cells is paralleled by a drop in particle density, which has also been observed in other *Rhodospirillaceae* (14, 37).

The incremental change in the size classes of particles in the photosynthetic membranes indicates that a unit of discrete size is being added to a core particle. Membrane particle size can be related to molecular weight via particle volume calculations and protein density in grams per cubic centimeter. Using 7.5 nm for the thickness of the membrane and the parameters of McDonnel and Staehelin (22) given in Table 3, we made the following estimations of molecular-weight ranges: 166,000 to 193,000 for a 7.5-nm spherical particle, 443,000 to 514,000 for a 10.0-nm cylindrical particle, 692,000 to 803,000 for a 12.5-nm cylindrical particle, 993,000 to 1,152,000 for a 15.0-nm cylindrical particle. Cylindrical volumes are used for the large particles due to the constraint of keeping the particle within the thickness of the membrane, by maintaining a constant height (7.5 nm) and increasing the particle diameter.

Firsow and Drews (8) have isolated the LHI and LHII complexes of *R. palustris* and, using polyacrylamide gel electrophoresis, have determined minimum molecular weights of 13,000 for LHI and approximately 20,000 for LHII peptides. Since polyacrylamide gel electrophoresis may not accurately estimate the weight of hydrophobic polypeptides (7, 46) and does not take into account the pigment contained in the complex, we will use slightly higher molecular weights for our proposed model: 15,000 for LHI, 25,000 for LHII, and 90,000 for the RC. Using these values, we propose that the 7.5-nm particle consists of an RC and six LHI complexes as a core unit. The size increase to 10.0 nm would then be due to the addition of 12 LHII complexes to the core. The 12.5-nm particle would have 24 LHII complexes added to the core, and the 15.0-nm particle would have 36 LHII complexes plus the core. Table 3 summarizes the particle size-molecular weight relationships and the proposed composition of the particles. Figure 12 diagrams the proposed structural organization of the RC, LHI, and LHII in the photosynthetic membranes for different particle sizes. The large photosynthetic units would be intermixed with smaller core particles with little or no tightly bound LHII, particularly in moderate- to high-light-grown cells.

Evidence from a variety of sources indicates that the proposed model is a reasonable way to think about the organization of the RC, LHI, and LHII in photosynthetic membranes from structural, biochemical, and functional view-

TABLE 3. Particle size, calculated molecular weight, and proposed composition of PF_s particles

Particle shape	Particle diam (nm)	Calculated mol wt range[a]	Proposed composition	Estimated wt[b]
Spherical	7.5	166,000–193,000	RC + 6 LHI (core)	180,000
Cylindrical	10.0	443,000–514,000	Core + 12 LHII	480,000
Cylindrical	12.5	692,000–803,000	Core + 24 LHII	780,000
Cylindrical	15.0	993,000–1,152,000	Core + 36 LHII	1,080,000

[a] The molecular weight was calculated by the formula molecular weight = $N_p V$ where $p = 1.25 - 1.45$ g/cm^3, $N = 6.02 \times 10^{23}$, V = volume (height of the cylinder = 7.5 nm).
[b] M_r used: RC = 90,000; LHI = 15,000; LHII = 25,000.

points. It has been shown that the RC and LHI are coregulated and that LHII is added to the membranes as light levels decrease (8, 15, 37), which would account for the existence of a high proportion of 7.5-nm core particles at high light levels and of increasing numbers of large particles as light decreases.

The sixfold symmetry of LHI around the RC is supported by the work of Miller on *R. viridis* (24, 25). This organism has only one type of LH component in association with its RC (48), in analogy with the core unit proposed here. Freeze-fracture images of *R. viridis* ICMs reveal a hexagonal arrangement of components in these membranes, confirming early studies of Giesbrecht and Drews (11). The hexagonal particle lattice can also be seen in negatively stained preparations of isolated thylakoid membranes, and Miller (24, 25) has used optical diffraction and digital image filtering of such micrographs to elucidate the supramolecular organization of the particles. According to this model, the repeating unit, believed to correspond to a functional RC-LH complex, consists of a large central particle with six smaller subunits arranged around it. *R. palustris* differs from *R. viridis* in having the LHII antenna, in addition to the RC-LHI unit. The presence of this additional complex in the photosynthetic membrane of *R. palustris* probably prevents the RC-LHI complexes from forming a lattice as seen in *R. viridis* thylakoid membranes. It is interesting to note that work by Woese et al. (53) indicates that *R. palustris* and *R. viridis* are more closely related on an evolutionary scale than are *R. palustris* and *R. sphaeroides*; therefore, the sixfold symmetry proposed here may be a consequence of that relationship, with the LHII being a later acquisition for *R. palustris*.

The work of Shiozawa et al. with *R. capsulata* (40, 41) indicates that the smallest unit of LHII which retains a native spectrum is probably a tetramer (or possibly a trimer) of LHII stoichiometric units. We postulate that each LHII stoichiometric unit may have two hydrophobic bonding domains which must be occupied by two other units to form a stable complex with a native spectrum. In our proposed model, the bonding domains are occupied by other LHII complexes or the LHIs of the core. As long as the bonding domains of the LHII complexes are occupied, they would yield a native spectrum; in vitro, this is achieved by the association of two LHII dimers, whereas in vivo this is accomplished either by an association with other LHII units or by association with the core complex.

Energy-transfer considerations also make this model appealing. Fluorescence studies of the LHII of *R. sphaeroides* show that the energy transfer from carotenoid to Bchl is up to 100% efficient in wild-type cells (3). The next feature of our model, i.e., the transfer of energy from LHII to LHI, has been shown to be remarkably efficient by Hunter et al. (16) in that when LHII and LHI are associated in vitro, nearly all absorbed energy seems to be passed to LHI since LHI fluorescence is all that is detected. These investigators have also speculated that this is a reflection of the organization of the two antenna components in the membrane. Van Grondelle and Rijgersberg (50) have examined energy transfer between the pigments of the antennae and proposed that LHI surrounds the RC and LHII surrounds LHI for a stepwise transfer of energy from LHII to LHI to the RC. Our model lends structural support to the above proposals by a modification of the "lake" model. Monger and Parson (26) examined the lake versus "puddle" models in *R. sphaeroides* by fluorescence kinetics. They found the lake model to be more consistent with their results—that there are not discrete photosynthetic units as would be seen in a "puddle" arrangement, but rather a large pool of LHI surrounding and interacting with several RCs, and that the LHI pool is, in turn, surrounded by a large LHII lake. Superficially, the model that we propose for the photosynthetic unit of *R. palustris* seems to contradict the lake model of Monger and Parson. However, the two models may actually be more complementary than contradictory in nature. The large particles, 12.5 to 15.0 nm, which we propose as the photosynthetic units, are only seen in appreciable amounts in low-light cells. With moderate to high light conditions, the most prevalent particles are in the 7.5- to 10.0-nm size range

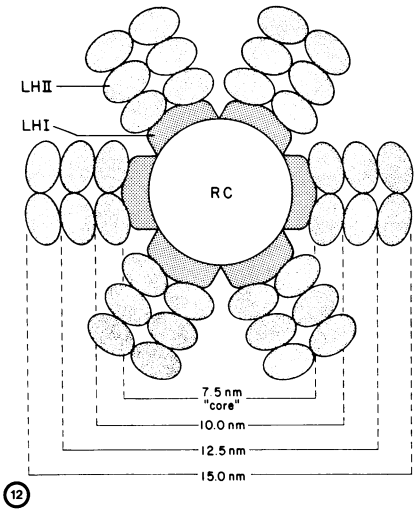

FIG. 12. Diagram of proposed organization of RC, LHI, and LHII in *R. palustris* photosynthetic membranes. The size of the complex varies with the amount of bound LHII, giving rise to particles on freeze-fractured membranes that fall into distinct size classes as indicated.

(Fig. 10), that is, the core (RC-LHI) particles. Other possible particles in this size range are core particles (7.5 nm) with additional LHI, rather than bound LHII. This abundance of core particles with high light conditions is consistent with a large LHI pool surrounding the RCs. Only when light becomes limiting (100 lx or less), do the discrete units of RC-LHI-LHII begin to be seen in significant numbers. But even at low light levels, a large proportion of 7.5- to 10.0-nm particles are present, suggesting that lake- and puddle-type organizations may coexist in the membrane. As more LHII is added to the membranes, more may become attached to the core particles, in addition to perhaps acting as a mobile energy carrier analogous to the mobile chlorophyll *a/b* light-harvesting component proposed for higher plants (20a). The model that we propose for the arrangement of LHII-LHI-RC of *R. palustris* bears a striking resemblance to the arrangement of the antenna-RC complexes seen in cyanobacteria and red algae, in that antennae are arranged for sequential absorbance and energy transfer down a line to the RC (10, 12). An analogous model has also been proposed for the relationship between antenna structures and RCs in green bacteria (45).

The proposal offered here does not preclude the possibility of some LHII existing as separate units (trimers or tetramers) in the membrane, perhaps with different geometry or stoichiometry than when associated with the core complex. The model is also accessible to testing if the larger particles (10.0 to 15.0 nm) can be isolated intact and examined for energy-transfer capabilities and protein and pigment composition.

ACKNOWLEDGMENTS

This work was supported by National Institute of General Medical Sciences grant GM 22912.

We thank Jan Logan for her excellent graphic artwork.

LITERATURE CITED

1. **Branton, D. S., S. Bullivant, N. G. Gilula, M. J. Karnovsky, H. Moor, K. Muhlentheler, D. Northcote, L. Packer, P. Satir, V. Speth, L. A. Staehelin, R. L. Steere, and R. S. Weinstein.** 1975. Freeze-etching nomenclature. Science **190**:54–56.
2. **Branton, D. S., and D. W. Deamer.** 1972. Membrane structure. Springer-Verlag, Vienna.
3. **Cogdell, R. J., M. F. Hipkins, W. MacDonald, and T. G. Truscott.** 1981. Energy transfer between the carotenoid and the bacteriochlorophyll within the B800-850 light-harvesting pigment-protein complex of *Rhodopseudomonas sphaeroides*. Biochim. Biophys. Acta **634**:191–202.
4. **Cohen-Bazire, G., W. R. Sistrom, and R. Y. Stanier.** 1957. Kinetic studies of pigment synthesis by non-sulfur purple bacteria. J. Cell Comp. Physiol. **49**:25–68.
5. **Drews, G.** 1978. Structure and development of the membrane system of photosynthetic bacteria. Curr. Top. Bioenerg. **8**:161–207.
6. **Drews, G., and P. Giesbrecht.** 1965. Die Thylakoidstrucuren von rhodopseudomonas spec. Arch. Mikrobiol. **52**:242–250.
7. **Feher, G.** 1971. Some chemical and physical properties of a bacterial reaction center particle and its primary photochemical reactants. Photochem. Photobiol. **14**:373–387.
8. **Firsow, N. N., and G. Drews.** 1977. Differentiation of the intracytoplasmic membranes of *Rhodopseudomonas palustris* induced by variations of oxygen partial pressure or light intensity. Arch. Microbiol. **115**:299–306.
9. **Frye, L. D., and M. Edidin.** 1970. The rapid intermixing of cell surface antigens after formation of mouse-human heterokaryons. J. Cell Sci. **7**:319–335.
10. **Gantt, E.** 1975. Phycobilisomes: light-harvesting pigment complexes. BioScience **25**:781–788.
11. **Giesbrecht, P., and G. Drews.** 1966. Uber die Organisation und die makromolekulare Architectur der thylakoide "lebendev" Bakterieu. Arch. Mikrobiol. **54**:297–330.
12. **Glazer, A. N.** 1980. Structure and evolution of photosynthetic accessory pigment systems with special reference to phycobiliproteins, p. 221–244. *In* D. Sigman and M. A. B. Brazier (ed.), Evolution of protein structure and function. Academic Press, Inc., New York.
13. **Golecki, J., G. Drews, and R. Buhler.** 1979. The size and number of intramembrane particles in cells of the photosynthetic bacterium *Rhodopseudomonas capsulata* studied by freeze-fracture electron microscopy. Cytobiologie **18**:381–389.
14. **Golecki, J. R., and J. Oelze.** 1980. Differences in the architecture of cytoplasmic and intracytoplasmic membranes of the chemotrophically and phototrophically grown species of the *Rhodospirillaceae*. J. Bacteriol. **144**:781–788.
15. **Golecki, J. R., A. Schumacher, and G. Drews.** 1980. The differentiation of the photosynthetic apparatus and the intracytoplasmic membrane in cells of *Rhodopseudomonas capsulata* upon variation of light intensity. Eur. J. Cell Biol. **23**:1–5.
16. **Hunter, C. N., R. A. Niederman, and R. K. Clayton.** 1981. Excitation energy transfer by antenna complexes isolated from *Rhodopseudomonas sphaeroides* by lithium dodecyl sulfate/polyacrylamide gel electrophoresis, p. 539–545. *In* G. Akoyunoglou (ed.), Photosynthesis. III. Structure and molecular organization of the photosynthetic apparatus. Balaban International Science Services, Philadelphia.
17. **Kaplan, S.** 1978. Control and kinetics of photosynthetic membrane development, p. 809–839. *In* R. Clayton and

W. Sistrom (ed.), The photosynthetic bacteria. Plenum Publishing Corp., New York.
18. **Kaplan, S.** 1981. Annual review: development of the membranes of photosynthetic bacteria. Photochem. Photobiol. **34**:769–774.
19. **Kaplan, S., and C. J. Arntzen.** 1982. Photosynthetic membrane structure and function, p. 65–153. *In* Govinjee (ed.), Photosynthesis: comparative aspects of bacteria and green plants. Academic Press, Inc., New York.
20. **Knoll, G., G. Oebel, and H. Plattner.** 1982. A simple sandwich-cryogen-jet procedure with high cooling rates for cryofixation of biological materials in the native state. Protoplasma **111**:161–176.
20a. **Kyle, D. J., L. A. Staehelin, and C. J. Arntzen.** 1983. Lateral mobility of the light-harvesting complex in chloroplast membranes controls excitation energy distribution in higher plants. Arch. Biochem. Biophys. **222**:527–541.
21. **Lommen, M. A. J., and J. Takemoto.** 1978. Ultrastructure of carotenoid mutant strain R-26 of *Rhodopseudomonas sphaeroides*. Arch. Microbiol. **118**:305–308.
22. **McDonnel, A., and L. A. Staehelin.** 1980. Adhesion between liposomes mediated by the chlorophyll a/b light-harvesting complex isolated from chloroplast membranes. J. Cell Biol. **84**:40–56.
23. **Merrick, J. M.** 1978. Metabolism of reserve materials, p. 199–219. *In* R. Clayton and W. Sistrom (ed.), The photosynthetic bacteria. Plenum Publishing Corp., New York.
24. **Miller, K. R.** 1979. Structure of a bacterial photosynthetic membrane. Proc. Natl. Acad. Sci. U.S.A. **76**:6415–6419.
25. **Miller, K. R.** 1982. Three-dimensional structure of a photosynthetic membrane. Nature (London) **300**:53–55.
26. **Monger, T. G., and W. W. Parson.** 1977. Singlet-triplet fusion in *Rhodopseudomonas sphaeroides* chromatophores. Biochim. Biophys. Acta **460**:393–407.
27. **Mullet, J. E., and C. J. Arntzen.** 1980. Simulation of grana stacking in a model membrane system. Mediation by a purified light harvesting pigment-protein complex from chloroplasts. Biochim. Biophys. Acta **589**:100–117.
28. **Nanninga, N.** 1971. The mesosome of *Bacillus subtilis* as affected by chemical and physical fixation. J. Cell Biol. **48**:219–224.
29. **Niederman, R. A., and K. D. Gibson.** 1978. Isolation and physicochemical properties of membranes from purple photosynthetic bacteria, p. 78–118. *In* R. Clayton and W. Sistrom (ed.), The photosynthetic bacteria. Plenum Publishing Corp., New York.
30. **Niederman, R. A., C. N. Hunter, G. S. Inamine, and D. E. Mallon.** 1981. Development of the bacterial photosynthetic apparatus, p. 663–674. *In* G. Akoyunoglou (ed.), Photosynthesis. V. Chloroplast development. Balaban International Science Services, Philadelphia.
31. **Parks, L. C., and R. P. Niederman.** 1978. Membranes of *Rhodopseudomonas sphaeroides*. V. Identification of bacteriochlorophyll *a*-depleted cytoplasmic membrane in phototrophically grown cells. Biochim. Biophys. Acta **511**:70–82.
32. **Pfennig, N.** 1978. General physiology and ecology of photosynthetic bacteria, p. 3–18. *In* R. Clayton and W. Sistrom (ed.), The photosynthetic bacteria. Plenum Publishing Corp., New York.
33. **Rash, J. E., and C. S. Hudson (ed.).** 1979. Freeze-fracture: methods, artifacts, and interpretations. Raven Press, New York.
34. **Reed, D. W., and D. Raveed.** 1972. Some properties of the ATPase from chromatophores of *Rhodopseudomonas sphaeroides* and its structural relationship to the bacteriochlorophyll proteins. Biochim. Biophys. Acta **283**:79–91.
35. **Sato, T.** 1968. A modified method for lead staining of thin sections. J. Electron Microsc. **17**:158.
36. **Scandella, C. J., P. Devaus, and H. M. McConnell.** 1972. Rapid lateral diffusion of phospholipids in rabbit sarcomplasmic reticulum. Proc. Natl. Acad. Sci. U.S.A. **69**:2056–2060.
37. **Schumacher, A., and G. Drews.** 1979. Effects of light intensity on membrane differentiation in *Rhodopseudomonas capsulata*. Biochim. Biophys. Acta **547**:417–428.
38. **Scolnik, P. A., D. Zannoni, and B. L. Marrs.** 1980. Spectral and functional comparisons between the carotenoids of the two antenna complexes of *Rhodopseudomonas capsulata*. Biochim. Biophys. Acta **593**:230–240.
39. **Shepherd, W. D., S. Kaplan, and J. T. Park.** 1981. Penicillin-binding proteins of *Rhodopseudomonas sphaeroides* and their membrane localization. J. Bacteriol. **147**:354–362.
40. **Shiozawa, J., P. Cuendet, H. Zuber, and G. Drews.** 1981. The light-harvesting B800-850 complex of *Rhodopseudomonas capsulata*: analysis of the native complex and its subunits, p. 427–434. *In* G. Akoyunoglou (ed.), Photosynthesis. III. Structure and molecular organization of the photosynthetic apparatus. Balaban International Science Services, Philadelphia.
41. **Shiozawa, J., W. Welte, N. Hodapp, and G. Drews.** 1982. Studies on the size and composition of isolated light-harvesting B800-850 pigment-protein complex of *Rhodopseudomonas capsulata*. Arch. Biochem. Biophys. **213**:473–485.
42. **Staehelin, L. A.** 1976. Reversible particle movements associated with unstacking and restacking of chloroplast membranes. J. Cell Biol. **71**:136–158.
43. **Staehelin, L. A.** 1981. Freeze-fracture studies of green plant and *Prochloron* thylakoids. A status report, p. 3–14. *In* G. Akoyunoglou (ed.), Photosynthesis. III. Structure and molecular organization of the photosynthetic apparatus. Balaban International Science Services, Philadelphia.
44. **Staehelin, L. A., P. A. Armond, and K. R. Miller.** 1977. Chloroplast membrane organization at the supramolecular level and its functional implications. Brookhaven Symp. Biol. **28**:278–315.
45. **Staehelin, L. A., J. R. Golecki, R. C. Fuller, and G. Drews.** 1978. Visualization of the supramolecular architecture of chlorosomes (Chlorobium type vesicles) in freeze-fractured cells of *Chloroflexus aurantiacus*. Arch. Microbiol. **119**:269–277.
46. **Steiner, L. A., M. Y. Okamura, A. D. Lopes, E. Moskowitz, and G. Feher.** 1974. Characterization of reaction centers from photosynthetic bacteria. II. Amino acid composition of the reaction center protein and its subunits in *Rhodopseudomonas sphaeroides* R-26. Biochemistry **13**:1403–1410.
47. **Tauschel, H. D., and G. Drews.** 1967. Thylakoid Morphgenese bei *Rhodopseudomonas palustris*. Arch. Mikrobiol. **59**:381–404.
48. **Trosper, T. L., D. L. Benson, and J. P. Thornber.** 1977. Isolation and spectral characteristics of the photochemical reaction center of *Rhodopseudomonas viridis*. Biochim. Biophys. Acta **460**:318.
49. **Valkirs, G. E., and G. Feher.** 1982. Topography of reaction center subunits in the membrane of the photosynthetic bacterium *Rhodopseudomonas sphaeroides*. J. Cell Biol. **95**:179–188.
50. **van Grondelle, R., and C. P. Rijgersberg.** 1981. Calculation of the B800-850 pigment-pigment distance in light-harvesting complexes of the purple bacteria *Rhodopseudomonas capsulata* (strain Y5), *Rhodopseudomonas sphaeroides*, Ga, and *Rhodopseudomonas sphaeroides* 3-4-1, p. 477–484. *In* G. Akoyunoglou (ed.), Photosynthesis. III. Structure and molecular organization of the photosynthetic apparatus. Balaban International Science Services, Philadelphia.
51. **Wakim, B., M. Schrader, and J. Oelze.** 1979. Characterization of cell-envelope fractions of chemotrophically and phototrophically grown *Rhodospirillum tenue*. Arch. Microbiol. **123**:287–293.
52. **Whittenburry, R., and A. G. McLee.** 1967. *Rhodopseudomonas palustris* and *Rhodopseudomonas viridis*. The photosynthetic budding bacteria. Arch. Mikrobiol. **59**:324–334.
53. **Woese, C. R., J. Gibson, and G. E. Fox.** 1980. Do genealogical patterns in purple photosynthetic bacteria reflect interspecific gene transfer? Nature (London) **283**:212–214.